

Review

# Recent Advances in the Structural Design of Silicon/Carbon Anodes for Lithium Ion Batteries: A Review

Yanan Mei<sup>1</sup>, Yuling He<sup>1</sup>, Haijiang Zhu<sup>1</sup>, Zeyu Ma<sup>2</sup>, Yi Pu<sup>1</sup>, Zhilin Chen<sup>1</sup>, Peiwen Li<sup>1</sup>, Liang He<sup>2</sup> , Wenwu Wang<sup>2</sup> and Hui Tang<sup>1,\*</sup><sup>1</sup> School of Materials and Energy, University of Electronic Science and Technology, Chengdu 611731, China<sup>2</sup> School of Mechanical Engineering, Sichuan University, Chengdu 610065, China

\* Correspondence: tanghui@uestc.edu.cn; Tel.: +86-18782917701

**Abstract:** As the capacity of lithium-ion batteries (LIBs) with commercial graphite anodes is gradually approaching the theoretical capacity of carbon, the development of silicon-based anodes, with higher energy density, has attracted great attention. However, the large volume variation during its lithiation/de-lithiation tends to lead to capacity decay and poor cycling performance. While rationally designed silicon/carbon (Si/C) anodes can exhibit higher specific capacity by virtue of silicon and high electrical conductivity and volume expansion suppression by virtue of carbon, they still show poor cycling performance with low initial coulombic efficiency. This review focuses on three strategies for structural design and optimization of Si/C anodes, i.e., carbon-coated structure, embedded structure and hollow structure, based on the recent researches into Si/C anodes and provides deeper insights into the problems that remain to be addressed.

**Keywords:** lithium-ion batteries; anode; silicon/carbon; structural design; electrochemical performance



**Citation:** Mei, Y.; He, Y.; Zhu, H.; Ma, Z.; Pu, Y.; Chen, Z.; Li, P.; He, L.; Wang, W.; Tang, H. Recent Advances in the Structural Design of Silicon/Carbon Anodes for Lithium Ion Batteries: A Review. *Coatings* **2023**, *13*, 436. <https://doi.org/10.3390/coatings13020436>

Academic Editors: Alexander Modestov and Torsten Brezesinski

Received: 29 November 2022

Revised: 28 January 2023

Accepted: 7 February 2023

Published: 15 February 2023



**Copyright:** © 2023 by the authors. Licensee MDPI, Basel, Switzerland. This article is an open access article distributed under the terms and conditions of the Creative Commons Attribution (CC BY) license (<https://creativecommons.org/licenses/by/4.0/>).

## 1. Introduction

Over the last decade, lithium-ion batteries (LIBs) have become an integral part of all types of electronic devices [1–4]. While the specific capacity of commercial graphite in LIBs is approaching its theoretical specific capacity (372 mAh g<sup>-1</sup>) [5,6], there is a growing demand for higher energy density. Currently, the main anodes available on the market include graphite, metal oxide and alloy, etc. Recently, numerous high-performance anodes are reported, such as spinel (Li<sub>4</sub>Ti<sub>5</sub>O<sub>12</sub>) composites [7], laminated Ti<sub>3</sub>C<sub>2</sub>T<sub>x</sub> (MXene) [8], and silicon-based anode [9].

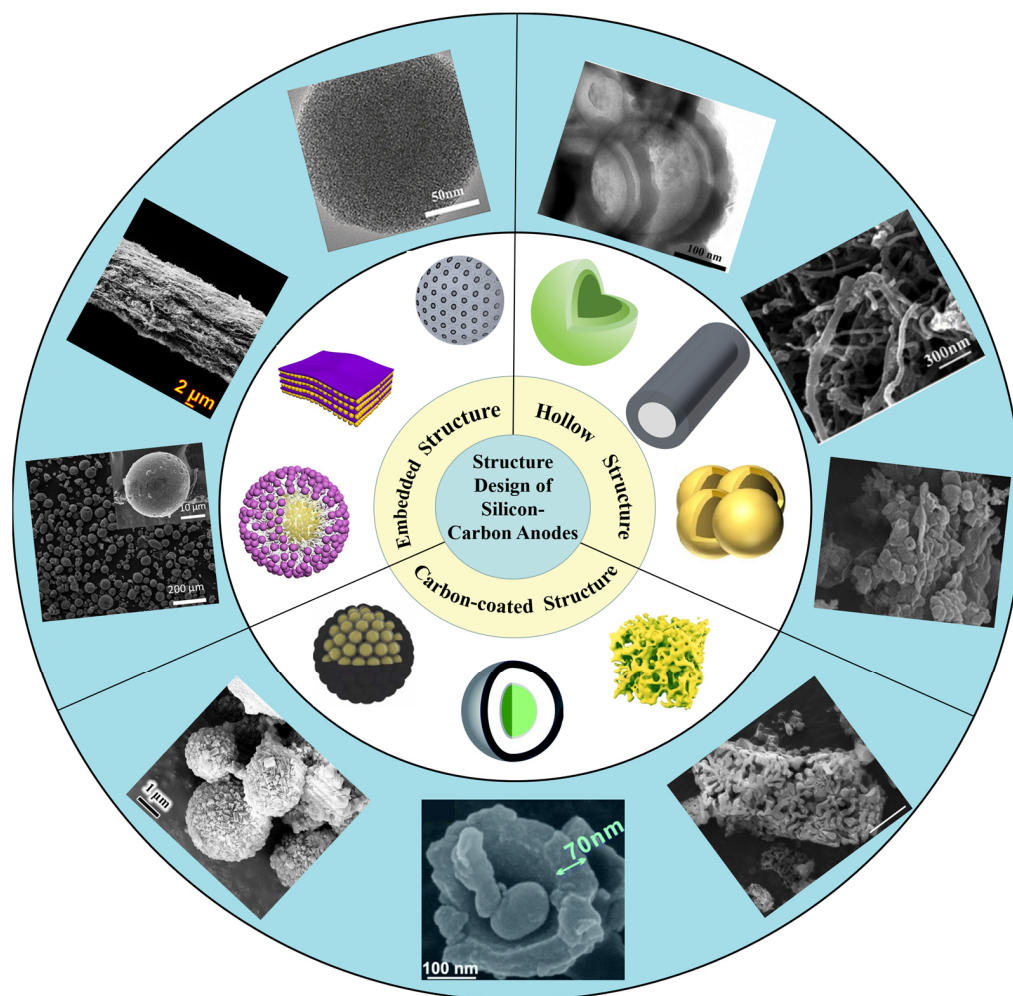
Silicon stands out due to its ultrahigh theoretical specific capacity (4200 mAh g<sup>-1</sup> [10]), which is 10 times that of a commercial graphite anode [11]. The silicon anode has a much richer source, lower de-lithiation potential, and better environmental friendliness compared with other anodes. However, silicon-based anodes face numerous limitations. For instance, during lithiation/de-lithiation [12], the huge volume expansion (up to 400% [13]) can generate great mechanical stress, fractures, and pulverization of the silicon particles after several cycles which seriously hinders the transport of lithium ions in the anode. This leads to electrode polarization, solid electrolyte interphase (SEI) film's reconstruction [14,15], low coulombic efficiency, and continuous capacity decay. Additionally, the SiO<sub>x</sub> electrode [16] as LIB anode can generate an inactive lithium silicate phase during the first cycle of irreversible charging and discharging, which can severely reduce the initial coulombic efficiency of the LIB and affect the electrical conductivity of the whole electrode [17]. Furthermore, the existing preparation methods of silicon-based anodes are complicated, costly, and cannot be used in industry [18–20].

Strategies such as silicon/carbon (Si/C) compositing, nano-structuring silicon [21–23], and manufacturing new binders and electrolytes [24,25] can help to overcome the limitations of the silicon-based anodes. Among them, the Si/C composite is widely studied due

to its high operability. Carbon materials show high cycling stability and high electrical conductivity. Therefore, compounding silicon with carbon will provide high specific capacity, and obtain significantly improved electrical conductivity of anode [26–28]. Additionally, as a buffer for the silicon anode, the outer carbon shell can prevent direct contact between electrolyte and silicon [29], forming a stable SEI film and reducing the volume changes during charging and discharging. Thus, the silicon-based structure is less likely to be destroyed and the structural integrity of the electrode is maintained [30]. The combination of silicon and carbon is very promising because they mutually compensate for the low specific capacity of carbon, and the mechanical instability and poor electrical contact of silicon [31]. Thus, the Si/C anodes show excellent lithiation and cycling stability [32].

The development of Si/C anodes began as early as 1995, when Dahn and co-workers used 11% atomic silicon embedded in pre-graphitic carbon [33]. Since then, significant researches were performed and the performance of the Si/C anodes was greatly improved. Following the development of silicon nanowires [34], Y. Cui and co-workers made an outstanding contribution to the structural design of Si/C anodes. In 2009, they developed nanowires with a Si/C core-shell structure [35]. In 2010, they developed carbon nanotube (CNT)-based silicon thin films [36], carbon nanofibers, and silicon nanowires as composite anodes [37] that lowered the weight of the electrode. In the following year, a silicon and carbon nano-coaxial sponge [38] was developed to increase the mass loading per unit area. To improve the industrial scalability, a yolk-shell structure that defined the void between “yolk” and “shell” [39] was developed in 2012, based on which a pomegranate structure [40] was also developed in 2014. Additionally, in 2012, a double-walled silicon nanotube anode [41] was developed based on silicon nanotubes, which significantly increased the charging rate. A carbon cladding structure [42] was developed in 2015. New structures were developed in 2016 like graphene and graphite in cladding [43] and embedded structures [44]. In addition, a conformal graphitic carbon/silicon/self-healing elastic polymer foam structure [45] was developed to meet the needs of stretchable materials. The main known methods to improve Si/C anodes are the structural design’s optimization and the preparation of high-performance binders [46,47] and electrolytes [48,49]. Structural optimization is favored by researchers because of the potential for diversity [50–53]. However, there are still some bottlenecks in the widespread commercialization of Si/C anodes. Therefore, to obtain a clear understanding of the optimal Si/C anodes, it is necessary to summarize the current status of the performance improvement in Si/C anodes by structure optimization and presenting a perspective.

This review summarizes the research development of three main structures, carbon-coated structure, embedded structure, and hollow structure (Scheme 1). Moreover, this review analyzes the problems of each structure and provides an outlook on the development direction of the Si/C anodes.



**Scheme 1.** Schematic diagram of different structures of Si/C composite anodes for lithium-ion batteries.

## 2. Carbon-Coated Structure

Since carbon-coated silicon-based anodes were proposed in the early 21st century [54], there are some important research results reported [55]. The main contribution of carbon coating is to enhance the electrical contact between the silicon particles, reduce electrode polarization, and improve the electrochemical performance of the assembled cell [56]. The carbon coating can also reduce the probability of direct contact between electrolyte and anode, inhibit the SEI's overgrowth, stabilize the interface, improve the coulombic efficiency, and prevent aggregation of silicon. The following subsections discuss the three main types of carbon-coated structures: core-shell structure, yolk-shell structure, and porous structure.

### 2.1. Core-Shell Structure

As early as 1999, Si/C anodes were reported as a core-shell structure composed of nano-silica powder and carbon black [57]. Conventional shell-layer structures usually have silicon nanoparticles (SiNPs) as the spherical core, with a layer of carbon encapsulated on the surface. However, in recent reports, various core-shell structures are reported such as those involving dimensional differences in the core, the multiple species of the shell, and heteroatom doping involved in the modification.

A new nanostructured Si/C anodes with enhanced lithium storage capacity and porous silicon microspheres@C core-shell structure (pSiMS@C) was proposed by Wang et al. [58]. The SiAl alloy was reacted with an organic acid under hydrothermal conditions by a facile self-corrosion method (Figure 1a). The SiAl/Al-MOF core-shell precursor was prepared, and the target product was synthesized by a series of annealing and etching

processes. The novel pSiMS@C core-shell structure is consisted of an amorphous carbon shell encapsulated by interconnected nanowires. This anode exhibited high electrochemical performance and provided a reversible capacity of 1027.8 mAh g<sup>-1</sup> after 500 cycles at 1 A g<sup>-1</sup>, with a high capacity retention of 79%. The pSiMS@C anode was an in-situ MOF-derived carbon shell, which could effectively improve the electrical conductivity of the anode and mitigate its volume expansion.

Li et al. [59] abandoned the conventional method of carbon shells encapsulating unmodified SiNPs. They designed a silicon/nitrogen-doped carbon layer/carbon skeleton microsphere (SCM) using a facile and economical electrospray technique. Each SiNP within the SCM was encapsulated by carbon and connected by a PAN skeleton (Figure 1b). Notably, in the microscopic morphological characterization result, more paths for electron transport are found, which were provided by the nitrogen-doped carbon layer on the surface of the SiNPs and the PAN-derived nitrogen-doped carbon skeleton (Figure 1c), which allowed the material to have high electrical conductivity. Additionally, the carbon layer sustained the stress of SiNPs during (de)lithiation, and the robust three-dimensional carbon skeleton maintained overall integrity. This material is similar to the Si/C anodes with a pomegranate-like shell structure developed by Cui et al. [40] in 2014. Both anodes exhibited excellent electrochemical performance, i.e., a high reversible specific capacity of 746 mAh g<sup>-1</sup> after 200 cycles, thus demonstrating the feasibility of this structure and potential for commercial applicability since the low cost of electrospray technology.

While the abovementioned core-shell structures exhibited high electrochemical performance, they still face critical challenges. For instance, the proper thickness of the carbon shell poses an important effect on buffering the expansion/extraction of the silicon core during the cycling process. Increasing the thickness helps reducing internal stress and avoid outer layer rupture. An excessively thick layer increases the weight of the anode, and the capacity of the nanocomposite anode is lowered due to the low lithium storage capacity of carbon [60]. Therefore, non-cracking and highly conductive shell layers are essential for core-shell structured Si/C anodes. A flexible N-doped freestanding core-shell Si/C nanofiber (SC-NF) anode reported by Li et al. [61] was prepared using a dual-coaxial electrostatic spinning and carbonization. The transmission electron microscope (TEM) image of this fiber structure (Figure 1d) shows that the Si particles are encapsulated by the carbon shell of the fiber, thus solving the problem of electrode's structural failure and alleviating the volume expansion of silicon. Notably, the binder-free core-shell structure has advantages over commercial binders, i.e., polyvinylidene fluoride and sodium carboxymethylcellulose, which are unable to suppress the drastic change in the volume of SiNPs during repeated cycling. Additionally, such a structural design simplifies the battery's assembly process and allows the homogenization process to be omitted when assembling coin-type batteries. In addition, such a one-dimensional structure brings high electrochemical performance to this anode. In the cycling curves of SC-NF-0, SC-NF-0.18, SC-NF-0.24, and SC-NF-0.30 electrodes at 0.5 A g<sup>-1</sup>, the SC-NF-0.24 has the best performance with an initial specific discharge capacity of 1441 mAh g<sup>-1</sup>.

Therefore, different types of core-shell structures, in terms of core form, fabrication process, and dimensionality, are reported in recent studies. While the core-shell structure is the first Si/C composite structure to be used, the electrochemical performance is often affected by the nonuniformity of the carbon coating. Additionally, modified core-shell structures have started to make a breakthrough in electrochemical performance, showing reversible capacity over 1000 mAh g<sup>-1</sup> after 500 cycles at 1 A g<sup>-1</sup>.

## 2.2. Yolk-Shell Structure

Yolk-shell structure differs from the core-shell structure with an additional artificially formed gap between the core and shell. With the yolk-shell structure, the volume expansion of silicon particles inside the shell can be accommodated by the engineered cavity. Furthermore, the conductive shell allows the transport of lithium ions and electrons, and provides a stable interface for good contact between the various particles, leading to a stable SEI

layer. Different yolk-shell structures with different electrochemical performances can be obtained using various synthesis methods. As early as 2012, Y. Cui and co-workers [39] had already conducted research on the yolk-shell structured Si/C (YS-Si/C) anode. In this structure, SiNPs (about 100 nm) were attached to the “yolk” of amorphous carbon (carbon layer with a thickness of 5–10 nm) as a fixed side of the “shell”, with voids on the corresponding side. The yolk structure has several advantages. Firstly, the gap between the carbon shell and SiNPs is significantly increased, allowing volume variations without affecting the electrode performance. Secondly, the integrity of the carbon shell prevents the electrolyte from coming into direct contact with the SiNPs. Thirdly, the electrical conductivity of the carbon shell structure improves the electrochemical performance. Fourthly, this fixed structure maintains the integrity of the microstructure inside the electrode. However, further studies have shown that the large voids in this structure cause a decrease in the bulk energy density and that the outer carbon shell is brittle.

Recently, Zhang et al. [62] proposed a new YS-Si/C anodes containing carbon-encapsulated rigid SiO<sub>2</sub> as the shell, multiple SiNPs as the yolk, and a flexible CNT network embedded with Fe<sub>2</sub>O<sub>3</sub> nanoparticles as the filler (Figure 1e). The gaps brought by the fillers (Fe<sub>2</sub>O<sub>3</sub> nanoparticles and CNTs) in YS-Si/C anodes have additional anode's reversible capacity for the electrode and increase the tap density. The carbon-coating by rigid SiO<sub>2</sub> provides greater mechanical strength than a thin carbon shell, improving the safety of the electrode. This anode exhibited excellent electrochemical performance when assembled with a commercially available cathode (Figure 1f).

Hu et al. [63] proposed a new type of double-shell layer yolk-shell structure (TSC-PDA-B) by encapsulating many small-sized SiNPs into a bilayer porous silicon shell (Figure 1g) through the strong etching effect of HF. The double-shell layer exhibited higher mechanical strength and electrical conductivity than the single-shell layer. Notably, this structure resulted in a large improvement in the lithium storage performance, i.e., a high initial capacity of 2108 mAh g<sup>-1</sup> at a current density of 100 mA g<sup>-1</sup> and superior cycling performance of 1113 mAh g<sup>-1</sup> over 200 cycles, which is attributed to the large specific surface area provided by many SiNPs.

However, HF is not environmentally friendly and the etching of the SiO<sub>2</sub> layer needs to be controlled very precisely to obtain satisfactory results. Huang et al. [64] proposed an HF-free strategy using calcination to achieve the carbonization of the inner polymer, polystyrene (PS), and the formation of voids on the surface of the outer polymer, polyaniline (PANI), by exploiting the difference in carbon yield between the two layers of polymers that act as carbon sources grown on the surface of SiNPs (Figure 1h). A thin carbon layer, attached to the surface of the external polymer (PANI), is employed as an eggshell, as shown in the scanning electron microscope (SEM) image of Si@C@void@C (Figure 1i). In Si@C@void@C, the low internal carbon yielding polymer acts as a pore provider and the high carbon yielding external polymer acts as a shell, both of which compensate each other for the formation of a complete yolk-shell structure. Thus, the cladding of PS and SiNPs is a promising strategy.

According to recent studies on the YS-Si/C anode, the gap can help alleviating the volume expansion of silicon. The electrochemical performance of the yolk-shell structure is further enhanced through various designs. However, some following important challenges remain, such as safety problems when the carbon eggshell is too thin, the increased resistance to lithium-ion transport when the eggshell is a rigid carbon layer, the toxic HF for etching, and the encapsulation of the inner polymer with SiNPs using polymers with different types of carbon obtained by calcination.

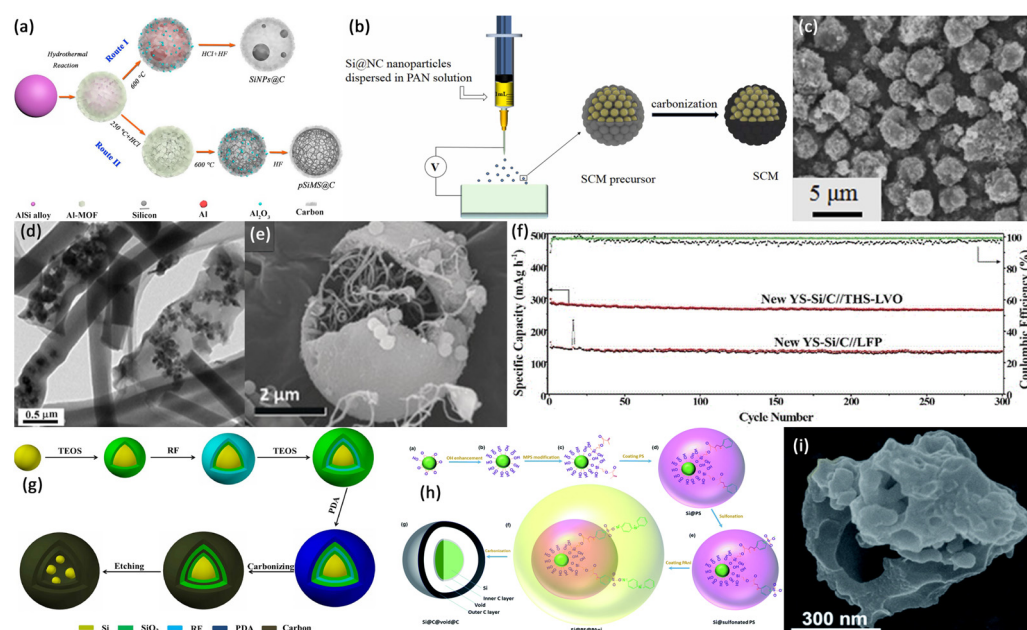


**Figure 1.** (a) Schematic illustration for the fabrication of SiNPs@C (Route I) and pSiMS@C (Route II) core-shell composites using SiAl@Al-MOF as the precursor. Reproduced with permission [58]. Copyright 2018, Elsevier. (b) Schematic diagram of SCM composite by electro spray technique, and (c) SEM image of SCM. Reproduced with permission [59]. Copyright 2022, Elsevier. (d) TEM image of SC-NF. Reproduced with permission [61]. Copyright 2021, ACS Publications. (e) SEM image of YS-Si/C anode, and (f) rate performance of the full cells of YS-Si/C anode//LFP. Reproduced with permission [62]. Copyright 2019, Wiley Online Library. (g) Schematic illustration of the preparation process of YS-Si/C composites. Reproduced with permission [63]. Copyright 2019, Elsevier. (h) Schematic illustration of the synthesis of the Si@C@void@C, and (i) SEM image of Si@C@void@C. Reproduced with permission [64]. Copyright 2018, Royal Society of Chemistry.

### 2.3. Porous Structure

The mechanism of the porous structure is similar to that of the yolk-shell structure, and the silicon's volume expansion is relieved by the introduction of voids in the structure. Unusually, the porous structure allows for an increase in the specific surface area of the silicon anode, allowing for easier diffusion of lithium ions, and thus increasing the reactivity of the anode. However, larger voids and porous structures caused the compressive strength of the particles to be decreased significantly, leading to poor structural integrity and electrochemical performance. Therefore, it is necessary to rationally design a porous structure with optimal voids and densities, so that the Si/C anodes have a large energy density, high initial coulombic efficiency, and long cycling stability [65].

To solve the difficulties of scalable synthesis of silicon-based anodes, An et al. [66] reported an ant nest-like microscale porous silicon (AMPSi), consisting of three-dimensionally interconnected silicon nano-microspheres and bicontinuous nanopores. A reasonable nanopore structure was produced by a top-down scalable method (Figure 2a), which led to a higher electrochemical performance of the target product, as shown by the carbon-coated AMPSi anode that retains up to 90% capacity after 1000 cycles. It is worth noting that such a structure can achieve a self-volume inward expansion mechanism, combining the advantages of Si, both nanoscale and microscale. The expansion of the AMPSi@C electrode's thickness is decreased to 20% during cycling, which is a qualitative improvement compared with the volume expansion of 300% in pure silicon electrodes.

Chen et al. [67] successfully prepared a scalable mesoporous ultrathin two-dimensional silicon nanosheet by a magnesium thermal reduction method (Figure 2b), and overcame the experimental difficulties caused by the non-van der Waals structure of silicon (simultaneous implementation of two-dimensional and mesoporous structures). The unique mesoporous

structure of the target product increased the specific surface area to  $386.2 \text{ m}^2 \text{ g}^{-1}$ , thus reducing the magnitude of volume expansion and increasing the contact area between the anode and the electrolyte. Furthermore, the two-dimensional sheet structure accelerated the diffusion of lithium ions and reduced the structural stress. Thus, this method offers the possibility to attain economically scalable two-dimensional mesoporous materials.

The porous structure is also easily derived from the natural biomass porous structure. Xu et al. [68] used biomass derived from soybean as the carbon and nitrogen source to overcome the complicated preparation process and high cost of the Si/N doped carbon composites (Figure 2c), and the synthesized Si@NN-BC-25 composite anode showed excellent electrochemical performance. The SiNPs in Si@NN-BC-25 were tightly wrapped in an amorphous carbon conductive network doped with nitrogen (Figure 2d), also known as a tofu gel matrix, resulting in “silicon tofu”. Herein, nitrogen doping provides more active sites for lithium-ion adsorption, and the tofu structure has high porosity and low bulk density, which effectively mitigate the volume expansion of silicon and prevent direct contact with the electrolyte. The Si@NN-BC-25 composite maintained a reversible capacity of  $731.6 \text{ mAh g}^{-1}$  at  $1 \text{ A g}^{-1}$  after 300 cycles.

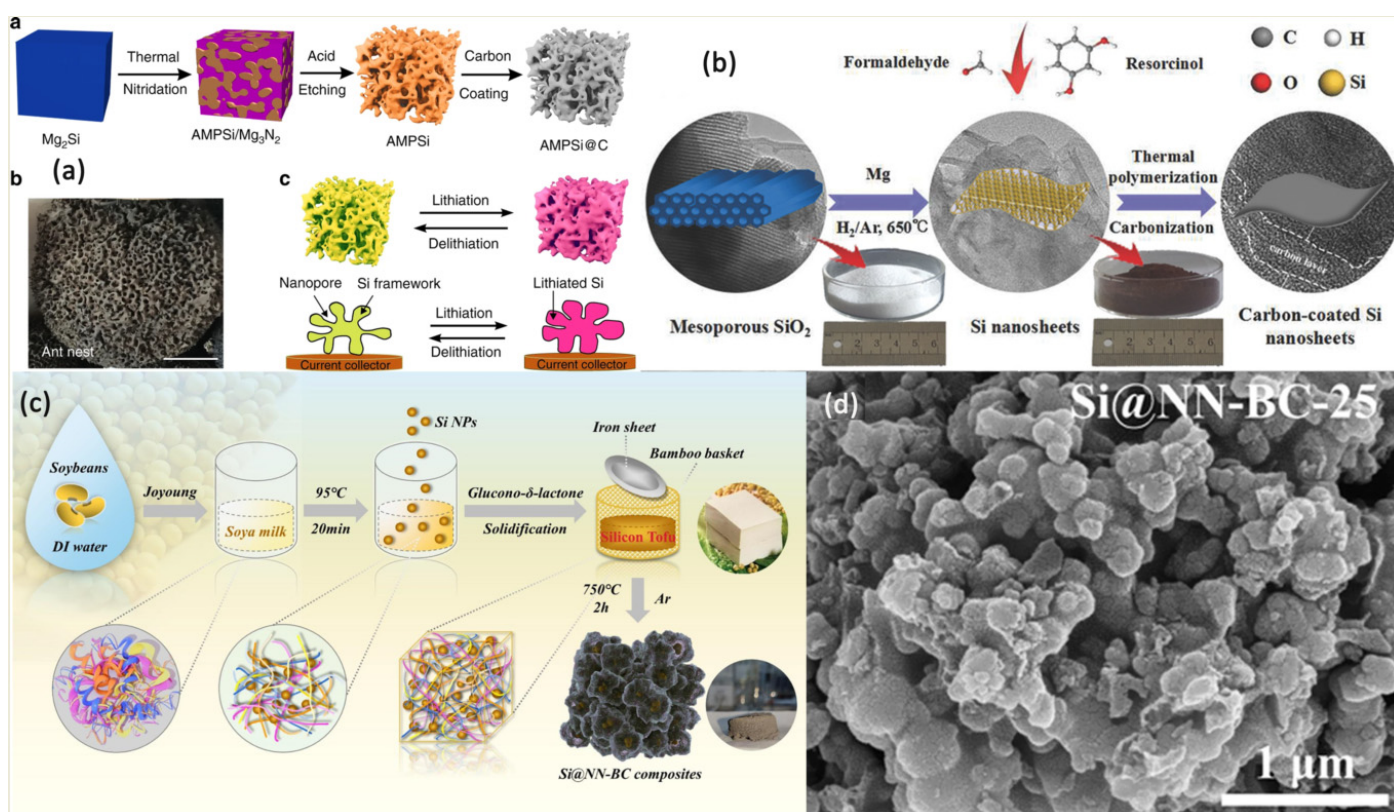


**Figure 2.** (a) Schematic diagram of AMPSi and AMPSi@C preparation and image of ant nests. Reproduced with permission [66]. Copyright 2019, Nature Communications. (b) Schematic illustration of the synthesis of nanosheets (inset: the large-scale products of  $\text{SiO}_2$  precursors (1.5 g) and Si nanosheets (0.63 g) synthesized one time). Reproduced with permission [67]. Copyright 2018, Wiley Online Library. (c) Schematic synthesis of the Si@NN-BC composites derived from silicon tofu, and (d) SEM images of Si@NN-BC-25. Reproduced with permission [68]. Copyright 2021, ACS Publications.

Conventional porous structures can be classified as follows [69], carbon layer covered with porous silicon, SiNPs dispersed in the porous carbon base, and porous carbon covered with porous silicon. In recent studies, porous materials were developed through dopant modification [70], different scales and dimensions, types of wrapping agents [71], and difference in the production process [72]. Biomass-derived carbon also attracts attention because of its natural porous structure [73]. In addition to the “silica tofu” mentioned

above, diatomaceous earth [74] was studied. However, some problems remain such as the complicated and expensive fabrication processes and environmental unfriendliness.

In summary, there are three types of carbon-coated structures, core-shell structure, yolk-shell structure, and porous structure. The carbon cladding provides reactive sites and alleviates volume expansion, which ensures the improved electrochemical activity of the silicon-based anodes. In a core-shell structure the outer carbon shell will relieve the volume expansion, and the thin carbon layer is prone to be broken during cycling. For the yolk-shell structure, the artificially added voids can compensate for the lack of the core-shell structure by allowing the expansion of the inner SiNPs to be largely relieved. The porous structure is unlike the others, which usually have a three-dimensional structure and a two-dimensional mesoporous structure. Such a porous structure has a large specific surface area, and the volume expansion of SiNPs is relieved [75,76]. Carbon-coated structure is one important structure applied to the design of Si/C anodes. Although the development of carbon coating in recent years presents a diversified trend, there are still some limitations such as uniform carbon coating, easy desorption of porous carbon coating, reasonable carbon content [77], and other limitations that still need to be solved [78]. Overall, carbon-coated structures have a high potential for commercialization. However, some challenges remain.

### 3. Embedded Structure

Embedded Si/C composites are generally SiNPs embedded in a continuous carbon matrix [79] or porous carbon skeleton [80], and the embedding of different nanoparticles into the carbon shell to achieve enhancement [81,82]. The advantage of this structure is that it will successfully alleviate the agglomeration of SiNPs, which is observed in encapsulated structures. Additionally, the voids in the embedded structure provide space for the expansion of SiNPs, which can effectively alleviate the change in electrochemical performance due to volume expansion and provide a channel for the transport of lithium ions [83].

The existing commercial Si/C anodes, with the cycling performance of graphite-blended Si/C (Si/C@G), will be somewhat higher than those with core-shell Si/C [84]. Thus, embedded Si/C structures and silicon in continuous carbon matrices were studied widely. For instance, Kwon et al. [85] synthesized a high-performance Si/C anodes using a low-cost and scalable microemulsion method (Figure 3a), with SiNPs embedded in micro-scale amorphous carbon spheres (amorphous carbon spheres from corn starch), with an outer graphitic carbon coating prepared from corn starch as a biological precursor. The target product exhibited good extensibility and outstanding electrochemical performance when assembled with a commercially available cathode, showing a high capacity of  $1800 \text{ mAh g}^{-1}$ , high cycling stability of 80% capacity retention after 500 cycles (Figure 3b), and short charging time. These advantages broaden the upper limit of performance that can be achieved by SiNPs embedded in a continuous carbon matrix. Furthermore, Huang et al. [86] employed a biomass carbon source to make an embedded matrix, with SiNPs in a fluffy rice carbon/nano-Si@C (FRC/NP-Si@C) structure consisting of rice as the biomass carbon source. This anode showed high electrochemical performance even at high silicon content (60%).

Achieving uniform carbon distribution is challenging in Si/C anodes and can impact the coulombic efficiency during cycling. To achieve a uniform distribution of carbon at the atomic scale, Zhu et al. [87] selected a molecular precursor capable of containing both silicon and carbon precursors (one bridged organ alkoxysilane precursor  $(R'O)_3Si-R-Si(OR')_3$  (R: incorporated organic group)) (Figure 3c). A silicon-based composite consisting of the homogeneous atomic-scale distribution of carbon (ASD-SiOC) was used, prepared from benzene-bridged mesoporous organosilicons (PBMOs), by a facile sol-gel method. Additionally, this structure led successfully to the optimization of the electrochemical performance of the Si/C anodes. This structure differs from conventional embedding, which does not embed SiNPs into a continuous carbon matrix or carbon skeleton. Conversely, the silicon-based material was used as a skeleton to achieve a uniform distribution of carbon

at the atomic scale. This unique structure opens the door to a new field of embedded structures and provides guidance for subsequent, more comprehensive studies.

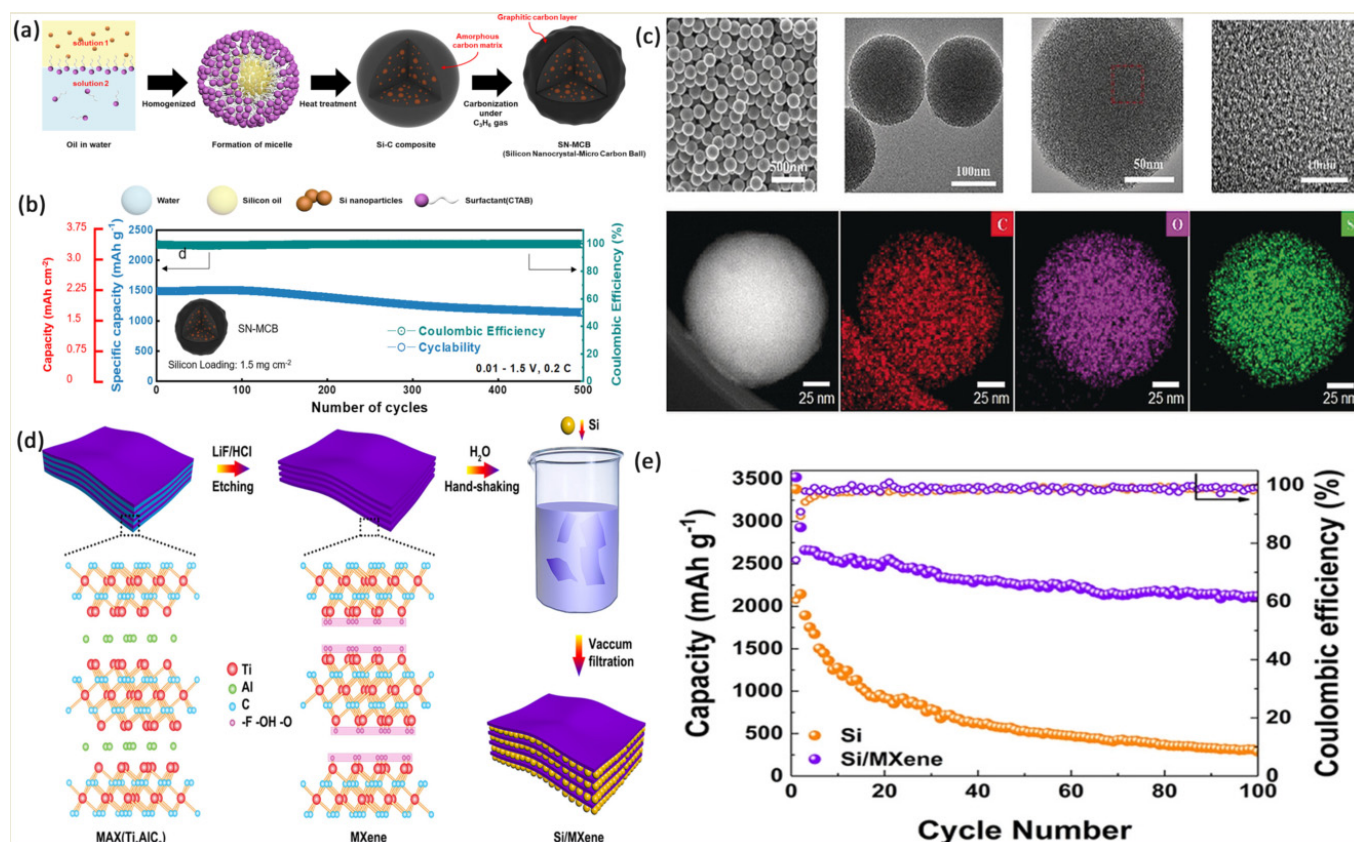


**Figure 3.** (a) Schematic Illustration of the synthesis of the proposed Si/C hybrid composite. Reproduced with permission [83]. Copyright 2019, ACS Publications. (b) Long-term cycling stability of the anodes in half-cells over a voltage range of 0.01–1.5 V at 0.2 C, and (c) the first row shows the field emission SEM images, TEM images and high-resolution TEM images of ASD-SiOC nanocomposites, and the second row shows the dark-field TEM images and corresponding elemental profiles of individual ASD-SiOC nanocomposite particles. Reproduced with permission [85]. Copyright 2019, Wiley Online Library. (d) The schematic diagram for preparing Si/MXene composite paper, and (e) cycling stability of Si/MXene and pure Si anodes at 200 mA·g<sup>-1</sup>. Reproduced with permission [86]. Copyright 2019, ACS Publications.

The layered interlayers in the hierarchical structure provide natural sites for the embedding of SiNPs. Among such materials, the hierarchical structure favored by researchers in recent years is MXene, a new two-dimensional transition metal carbide with excellent electrical, electrochemical and mechanical performance. The large specific surface area of MXenes provides greater possibilities for embedding SiNPs. For instance, Tian et al. [88] embedded SiNPs into the laminate structure based on the structure of the flexible Si/MXene composite paper (Figure 3d). The advantages of two components in the materials are combined in this structure. The SiNPs embedded between the layers prevent the failure of the active sites due to the overlapping of the MXene sheets, while the flexible MXene sheets mitigate the volume expansion of the active material during cycling, thus, reducing the rupture of SEI film. This embedded structure of MXene allows the anode to have high lithium storage and electrochemical performance, showing 2118 mAh g<sup>-1</sup> at 200 mA g<sup>-1</sup> after 100 cycles (Figure 3e). Hui et al. [89] used the embedded structure of MXene composites with SiNPs. They obtained a better dispersion morphology of SiNPs and a chemical bond between MXene and Si, with favorable reaction kinetics, while preventing the disruption of the two-dimensional Ti<sub>3</sub>C<sub>2</sub> MXene ultrathin layered structure. They developed

an efficient low-temperature homogeneous in-situ growth method with relatively mild conditions for coupling Si and MXene. Notably, the  $\text{Ti}_3\text{C}_2$  MXene shows a pseudocapacitive behavior, which contributes to the reversible capacity and makes the new layered porous MXene/Si nanocomposites with excellent electrochemical performance.

Conventional embedded Si/C anodes include embedding SiNPs into a continuous carbon matrix or carbon skeleton [90,91]. This embedding creates voids to achieve volume expansion mitigation, and the carbon matrix and the carbon skeleton are employed to obtain increased electrical conductivity, i.e., biomass-derived carbon as the carbon skeletons. However, embedded structures also present some challenges. Firstly, when SiNPs are embedded in the carbon skeleton after cycling, it is easy for the structure to break or detach, resulting in direct contact of the active material with the electrolyte which leads to continuous SEI growth and poor performance of the electrode. Secondly, the reversible capacity of the composite decreases when the Si: C ratio is increased [92]. In addition to conventional embedding structures, several embedding matrices can be investigated, such as the interlayer embedding mentioned above. However, more studies are needed because the fabrication processes involved in these strategies are complicated and commercially unavailable.

#### 4. Hollow Structure

Unlike the yolk-shell structure with artificially introduced voids, hollow structure usually doesn't have a nucleus in the interior of the microstructure [93]. However, most preparation methods for hollow structure are similar to those of yolk-shell structure and involve the template method. The hollow structure was widely studied because of its large internal void volume, which provides considerable relief from the stress-strain caused by the embedding of lithium ions. The thin shell brings the active material closer to the electrolyte, shortening the transport path of lithium-ion and improving the electrochemical performance [94–96]. Depending on the template's morphology, templates can be classified into hard templates (i.e., porous silicon templates, silicon microspheres, and MgO) and soft templates (i.e., gels, anti-gels, and vesicles, formed by aggregation of surfactant molecules). Herein, the hollow-structured Si/C composite anodes are classified according to the type of template used in the hollow structure.

##### 4.1. $\text{SiO}_2$ Template

The  $\text{SiO}_2$  as a template could be used to obtain hollow structures through a magnesium thermal reduction reaction. However, the SiC produced in this process will decrease the electrochemical performance of the anode. Li et al. [97] developed a SiC-free hollow Si/C anodes using  $\text{SiO}_2$  as a template through magnesium thermal reduction to obtain a porous Si@C ball-in-ball hollow structure. The porous Si@C hollow sphere structure generated by HCl etching of  $\text{Al}_2\text{O}_3$ , and the existence of reasonable voids between the carbon layer (Figure 4a) and the hollow structure are beneficial to alleviate the volume variation during cycling. The Si@C anode with this design showed excellent lithium storage performance, i.e., a capacity of  $813.2 \text{ mAh g}^{-1}$  at 0.1 C after 100 cycles.

Wang et al. [98] used natural reed extract as the Si source and  $\text{CO}_2$  as the carbon source, leading to a low cost since biomass feedstock. The concentration of HCl and content of  $\text{CO}_2$  had a significant impact on the composition, crystallinity, structure, electrical conductivity, specific surface area, pore volume, and particle distribution of the Si/C complexes. The optimal anode was obtained at 21 wt.% carbon and 3 M HCl, delivering a large reversible specific capacity of  $1548 \text{ mAh g}^{-1}$  at 100 mA  $\text{g}^{-1}$ . The development of this low-cost hollow structure paves a new path for the scalable preparation of Si/C composite anodes.

Jiang et al. [99] reported a Si/C composite prepared by  $\text{SiO}_2$  template and obtained a unique structure of a silicon layer encapsulated in a bilayer of elastic carbon cushioned hollow shell by a simple layer-by-layer assembly and magnesium thermal reduction method (Figure 4b). In this structure, the elastic carbon shells inside and outside can make the volume expansion of silicon adaptive in both internal and external directions, while the

hollow structure inside also stabilizes the mechanical performance. The electrode achieved a very high cycle life and reversible specific capacity.

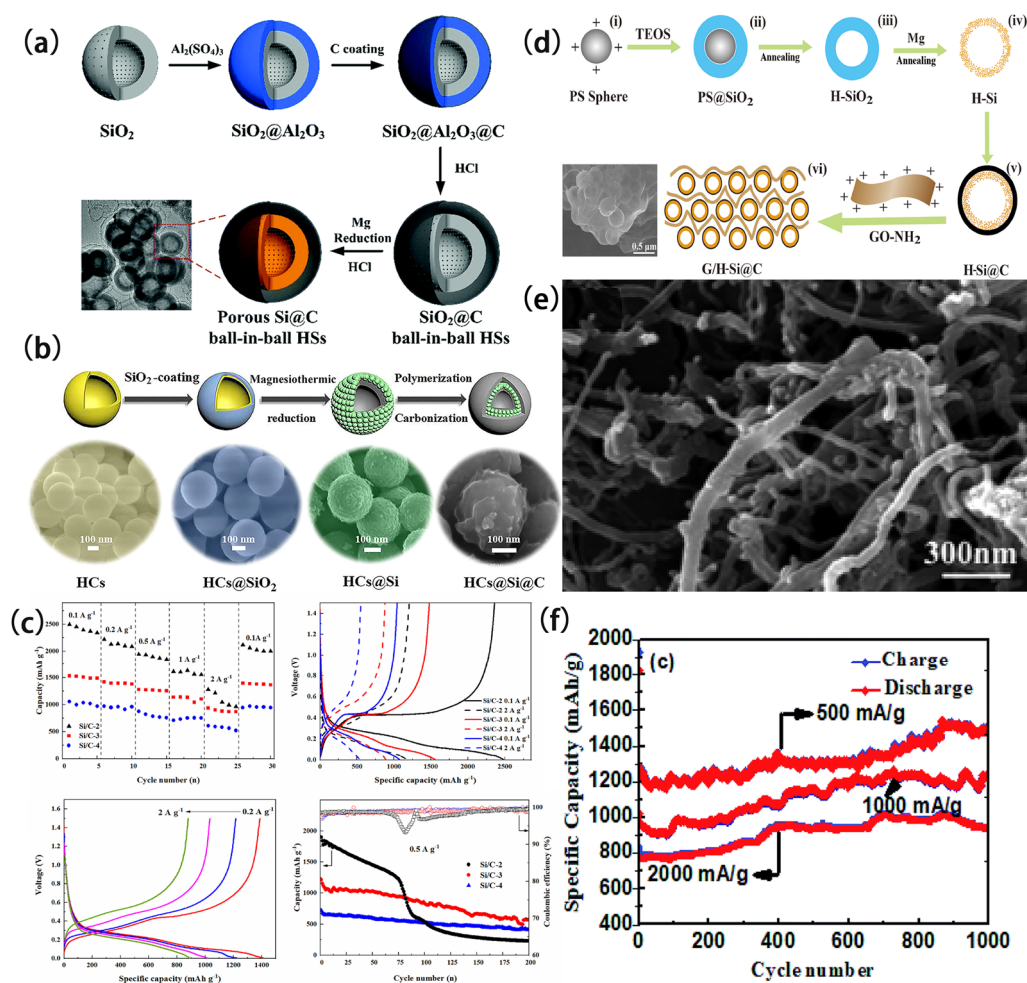


**Figure 4.** (a) Schematic fabrication process of porous Si@C ball-in-ball hollow spheres. Reproduced with permission [95]. Copyright 2018, Royal Society of Chemistry. (b) Schematic illustration of the synthesis processes of hollow carbon spheres (HCs)@Si@C "hollow triple-layer puff" structure. Reproduced with permission [97]. Copyright 2019, ACS Publications. (c) Rate capability, discharge-charge curve and cycling performance of different SiC hybrids. Reproduced with permission [98]. Copyright 2021, Elsevier. (d) Schematic illustration of producing G/H-Si@C bubble film composite structure. Reproduced with permission [99]. Copyright 2020, Elsevier. (e) SEM images of CNTs/Si/C, and (f) cycle performance of cells with CNTs/Si/C anodes at different current densities. Reproduced with permission [100]. Copyright 2018, Royal Society of Chemistry.

Preparing hollow Si/C structures using SiO<sub>2</sub> as a template has disadvantages. Firstly, the generation of SiC posed negative effects on the anode's electrochemical characteristics. Reducing the contact area between SiO<sub>2</sub> and the shell will prevent the generation of SiC. Secondly, the magnesium thermal reduction reaction requires a high temperature, causing difficulty in generating hollow structures. Thirdly, the gap between the hollow structure and the externally attached carbon layer needs to be moderate. The larger gap makes SiNPs agglomerate, which affects the electrochemical activity. In contrast, the smaller gap makes the volume expansion during cycling damage the carbon layer. The use of SiO<sub>2</sub> as a template for hollow structures, especially using cheaper biomass feedstock, is a feasible strategy. However, more studies are needed to achieve mass production.

#### 4.2. Self-Sacrificing Templates

In addition to SiO<sub>2</sub> as a template to provide a silicon source to make hollow structures, there is also a self-sacrificing template. HF or HCl etching is typically used to sacrifice the material for obtaining the hollow structure. The materials often used as self-sacrificing templates to make cavities are MgO, amino PS, polyethyleneimine (PEI), etc. Among these, the most representative one is the MgO template. For instance, Zhang et al. [100] removed the in-situ-generated MgO templates by acid etching to achieve a hollow structure. They used excess Mg vapor and CO<sub>2</sub> (green carbon source) to achieve an interconnected carbon network between SiNPs, which significantly improved the electrical conductivity and electron transfer during cycling. This high-rate, long-cycle life interconnected hollow Si/C nanosphere anode (Figure 4c) contained no insulating SiC and exhibited excellent electrochemical performance.

Amino PSs are also used as self-sacrificing templates. For instance, Liu et al. [101] prepared a flexible graphene bubble film@thin mesoporous carbon shell, encapsulating submicron level Si@C hollow sphere structures and using PS as a sacrificing template through a thermal treatment and chemical vapor deposition (Figure 4d). Notably, the compact structure resulted in a significantly reduced transport distance of electrons and lithium ions. The effect of the double-shell layer alleviates volume expansion of the silicon, enhances lithium storage, and controls the SEI's formation. Thus, the composite anode has a high initial coulombic efficiency.

The hollow structure is also closely related to the suppression of pulverization caused by repeated rupture of the SEI in the silicon anode during cycling. Specifically, the inner and outer layers of the hollow structure will expand outward during the process of lithium, resulting in repeated breakage of the SEI film and thus thickening the SEI layer, establishing an insulating layer, and making the silicon anode activity ineffective, which is exactly the inhibition behavior we mentioned. As early as 2012, Y. Cui and co-workers [41] developed a silicon hollow nanofiber structure based on a self-sacrificing carbon template method to prepare a surface layer of silicon that was reduced to SiO<sub>x</sub> during the annealing process, thus avoiding the problem of repeated breakage of the SEI film and leading to higher mechanical characteristics. In the last five years, hollow nanotube structures based on Si/C anodes have also been developed. For instance, Liu et al. [102] synthesized a sandwich-like carbon-coated coaxial core-shell CNTs/Si hollow nanofiber tube structure using CNTs as sacrificing template. In this structure, CNTs act as a perfect template for Si deposition, stabilizing the mechanical performance because of its sandwich-like hollow structure that can be observed in the microscopic form (Figure 4e). Both the CNTs and the carbon layer have a positive effect in achieving improved electrical conductivity of the CNTs/Si/C anode. Additionally, the target products still maintain good electrochemical characteristics. After long cycling, a stable reversible discharge capacity of CNTs/Si/C nanotubes of up to 1508.5 mA h g<sup>-1</sup> was obtained. The gradual increase in capacity will be attributed to the formation of a stable polymer gel layer resulting from kinetically activated electrolyte degradation (Figure 4f)

Self-sacrificing templates are constructed by growing silicon on the surface of the template, followed by thermal decomposition or acid etching of its components to achieve hollow structures. The electrochemical behavior of the hollow structure prepared by this method is determined by the surface shell structure, which can alleviate the expansion of the active material. Additionally, the fabrication procedure is usually unstable and scalable.

The cavity in the hollow structure is the highlight of this structural design [103], which plays the role of relieving the volume variations during cycling internally. Different templates play different roles in the structural design of the hollow structure, some acting as the silicon source and some acting as the cavity obtained after self-sacrifice. However, during the cavitation process, acid etching is usually unavoidable, and thus, more environmentally friendly ways need to be developed [104]. In addition, the hollow structure of Si/C anodes also faces the inhibition behavior caused by the repeated breaking of SEI film on the surface shell. In a word, hollow structures have more possibilities for structural modification. It can

also be found in the reported literature that the above problems can be solved by designing shells with different functional structures.

## 5. Conclusions

Silicon, a non-toxic material with abundant resources on earth and high theoretical capacity, is the ideal anode. However, commercialization of silicon anodes are limited due to their huge volume expansion and poor electrical conductivity. Hence, various strategies have been developed to overcome these limitations, such as designing electrolytes and Si/C anodes together through nano-structuring. In this review, based on the current state of research on structure optimization of Si/C anodes, we classified Si/C anodes into three categories, carbon-coated structure, embedded structure, and hollow structure. Moreover, the advantages and disadvantages of three types of Si/C anodes are summarized. However, these strategies still face challenges, which have been summarized as follows.

- (1) Attaining uniform coatings in the carbon-coated structure is still challenging, and uneven coating impacts the lithium-ion diffusion rate, leading to poor cycle life.
- (2) As the most developed structural optimization method, the carbon cladding includes a variety of strategies in terms of cladding content and cladding form. However, its impact on improving the overall electrochemical performance is still limited.
- (3) The loss of SiNPs in the embedded structure reduces the anode content, which affects the performance.
- (4) The fabrication of hollow structures usually involves templates and acid etching, which is not environmentally friendly.

The addition of carbon-based materials does not sufficiently address the challenges associated with the volume expansion of silicon-based anodes, the repeated fragmentation of SEI films, and the poor electrical conductivity. The following aspects should be attained in further studies.

- (1) A uniform carbon coating and an optimal ratio of Si: C.
- (2) More stable bonding when SiNPs are embedded.
- (3) More environmentally friendly methods of template removal and more non-toxic precursors.
- (4) Reasonable void and hole design, i.e., the more reasonable spacing between shell layers in hollow structures.

While the recently reported Si/C anodes have not reached the theoretical specific capacity of silicon ( $4200 \text{ mAh g}^{-1}$ ), the emergence of new processes and novel structures present promising electrochemical performance. As one of the silicon-based anodes most likely to be commercialized, Si/C anodes have the potential to replace commercial graphite anodes.

**Author Contributions:** Conceptualization, Y.M. and H.T.; investigation, Y.M., Y.H. and H.Z.; resources, Y.P. and Z.C.; writing—original draft preparation, Y.M.; writing—review and editing, Z.M., L.H. and W.W.; visualization, Y.P. and P.L.; supervision, H.T.; project administration, H.T.; funding acquisition, H.T. All authors have read and agreed to the published version of the manuscript.

**Funding:** This research was funded by the National Science and Technology Major Project (No. 2020YFB1506001), and the Department of Science and Technology of Sichuan Province (No. 2021YFG0231).

**Institutional Review Board Statement:** Not applicable.

**Informed Consent Statement:** Not applicable.

**Data Availability Statement:** All data that support the findings of this study are included within the article.

**Conflicts of Interest:** The authors declare no conflict of interest.

## References

1. Grey, C.P.; Hall, D.S. Prospects for lithium-ion batteries and beyond—a 2030 vision. *Nat. Commun.* **2020**, *11*, 6279. [[CrossRef](#)]
2. Li, M.; Lu, J.; Chen, Z.; Amine, K. 30 years of lithium-ion batteries. *Adv. Mater.* **2018**, *30*, 1800561. [[CrossRef](#)] [[PubMed](#)]
3. Liu, J.; Bao, Z.; Cui, Y.; Dufek, E.J.; Goodenough, J.B.; Khalifah, P.; Zhang, J.G. Pathways for practical high-energy long-cycling lithium metal batteries. *Nat. Energy* **2019**, *4*, 180–186. [[CrossRef](#)]
4. Zubi, G.; Dufo-López, R.; Carvalho, M.; Pasaoglu, G. The lithium-ion battery: State of the art and future perspectives. *Renew. Sustain. Energy Rev.* **2018**, *89*, 292–308. [[CrossRef](#)]
5. Wu, F.; Maier, J.; Yu, Y. Guidelines and trends for next-generation rechargeable lithium and lithium-ion batteries. *Chem. Soc. Rev.* **2020**, *49*, 1569–1614. [[CrossRef](#)]
6. Zhang, W.J. A review of the electrochemical performance of alloy anodes for lithium-ion batteries. *J. Power Sources* **2011**, *196*, 13–24. [[CrossRef](#)]
7. Yi, T.F.; Yang, S.Y.; Xie, Y. Recent advances of  $\text{Li}_4\text{Ti}_5\text{O}_{12}$  as a promising next generation anode material for high power lithium-ion batteries. *J. Mater. Chem. A* **2015**, *3*, 5750–5777. [[CrossRef](#)]
8. Xiong, D.; Li, X.; Bai, Z.; Lu, S. Recent advances in layered  $\text{Ti}_3\text{C}_2\text{T}_x$  MXene for electrochemical energy storage. *Small* **2018**, *14*, 1703419. [[CrossRef](#)]
9. Feng, K.; Li, M.; Liu, W.; Kashkooli, A.G.; Xiao, X.; Cai, M.; Chen, Z. Silicon-based anodes for lithium-ion batteries: From fundamentals to practical applications. *Small* **2018**, *14*, 1702737. [[CrossRef](#)]
10. Wen, C.J.; Huggins, R.A. Chemical diffusion in intermediate phases in the lithium-silicon system. *J. Solid State Chem.* **1981**, *37*, 271–278. [[CrossRef](#)]
11. Wu, H.; Cui, Y. Designing nanostructured Si anodes for high energy lithium ion batteries. *Nano Today* **2012**, *7*, 414–429. [[CrossRef](#)]
12. Zuo, X.; Zhu, J.; Müller-Buschbaum, P.; Cheng, Y.-J. Silicon based lithium-ion battery anodes: A chronicle perspective review. *Nano Energy* **2017**, *31*, 113–143. [[CrossRef](#)]
13. Cui, Y. Silicon anodes. *Nat. Energy* **2021**, *6*, 995–996. [[CrossRef](#)]
14. Lucas, I.T.; Pollak, E.; Kosteki, R. In situ AFM studies of SEI formation at a Sn electrode. *Electrochem. Commun.* **2009**, *11*, 2157–2160. [[CrossRef](#)]
15. Jiang, J.; Zhang, H.; Zhu, J.; Li, L.; Liu, Y.; Meng, T.; Ma, L.; Xu, M.; Liu, J.; Li, C.M. Putting Nanoarmors on Yolk-Shell Si@C Nanoparticles: A Reliable Engineering Way To Build Better Si-Based Anodes for Li-Ion Batteries. *ACS Appl. Mater. Interfaces* **2018**, *10*, 24157–24163. [[CrossRef](#)]
16. Li, Z.; He, Q.; He, L.; Hu, P.; Li, W.; Yan, H.; Peng, X.; Huang, C.; Mai, L. Self-sacrificed synthesis of carbon-coated  $\text{SiO}_x$  nanowires for high capacity lithium ion battery anodes. *J. Mater. Chem. A* **2017**, *5*, 4183–4189. [[CrossRef](#)]
17. Chen, T.; Wu, J.; Zhang, Q.; Su, X. Recent advancement of  $\text{SiO}_x$  based anodes for lithium-ion batteries. *J. Power Sources* **2017**, *363*, 126–144. [[CrossRef](#)]
18. Ma, C.; Wang, Z.; Zhao, Y.; Li, Y.; Shi, J. A novel raspberry-like yolk-shell structured Si/C micro/nano-spheres as high-performance anode materials for lithium-ion batteries. *J. Alloys Compd.* **2020**, *844*, 156201. [[CrossRef](#)]
19. Xu, Q.; Sun, J.-K.; Li, J.-Y.; Yin, Y.-X.; Guo, Y.-G. Scalable synthesis of spherical Si/C granules with 3D conducting networks as ultrahigh loading anodes in lithium-ion batteries. *Energy Storage Mater.* **2018**, *12*, 54–60. [[CrossRef](#)]
20. Zhang, W.; Wang, D.; Shi, H.; Jiang, H.; Wang, C.; Niu, X.; Yu, L.; Zhang, X.; Ji, Z.; Yan, X. Industrial waste micron-sized silicon use for Si@C microspheres anodes in low-cost lithium-ion batteries. *Sustain. Mater. Technol.* **2022**, *33*, e00454. [[CrossRef](#)]
21. Xu, Z.-L.; Liu, X.; Luo, Y.; Zhou, L.; Kim, J.-K. Nanosilicon anodes for high performance rechargeable batteries. *Prog. Mater. Sci.* **2017**, *90*, 1–44. [[CrossRef](#)]
22. Kabashin, A.V.; Singh, A.; Swihart, M.T.; Zvestovskaya, I.N.; Prasad, P.N. Laser-Processed Nanosilicon: A Multifunctional Nanomaterial for Energy and Healthcare. *ACS Nano* **2019**, *13*, 9841–9867. [[CrossRef](#)]
23. Su, Y.; Feng, X.; Zheng, R.; Lv, Y.; Wang, Z.; Zhao, Y.; Shi, L.; Yuan, S. Binary Network of Conductive Elastic Polymer Constraining Nanosilicon for a High-Performance Lithium-Ion Battery. *ACS Nano* **2021**, *15*, 14570–14579. [[CrossRef](#)] [[PubMed](#)]
24. Wen, Z.; Wu, F.; Li, L.; Chen, N.; Luo, G.; Du, J.; Zhao, L.; Ma, Y.; Li, Y.; Chen, R. Electrolyte Design Enabling Stable Solid Electrolyte Interface for High-Performance Silicon/Carbon Anodes. *ACS Appl. Mater. Interfaces* **2022**, *14*, 38807–38814. [[CrossRef](#)] [[PubMed](#)]
25. Li, Y.; Zhou, X.; Hu, J.; Zheng, Y.; Huang, M.; Guo, K.; Li, C. Reversible Mg metal anode in conventional electrolyte enabled by durable heterogeneous SEI with low surface diffusion barrier. *Energy Storage Mater.* **2022**, *46*, 1–9. [[CrossRef](#)]
26. Zhang, X.; Weng, J.; Ye, C.; Liu, M.; Wang, C.; Wu, S.; Tong, Q.; Zhu, M.; Gao, F. Strategies for Controlling or Releasing the Influence Due to the Volume Expansion of Silicon inside Si–C Composite Anode for High-Performance Lithium-Ion Batteries. *Materials* **2022**, *15*, 4264. [[CrossRef](#)] [[PubMed](#)]
27. Hsieh, C.-C.; Liu, W.-R. Effects of nitrogen doping on Si/carbon composite anode derived from Si wastes as potential active materials for Li ion batteries. *J. Alloys Compd.* **2019**, *790*, 829–836. [[CrossRef](#)]
28. Liu, S.; Xu, J.; Zhou, H.; Wang, J.; Meng, X. B-Doped Si@C Nanorod Anodes for High-Performance Lithium-Ion Batteries. *J. Nanomater.* **2019**, *2019*, 6487156. [[CrossRef](#)]
29. Jiang, M.; Ma, Y.; Chen, J.; Jiang, W.; Yang, J. Regulating the carbon distribution of anode materials in lithium-ion batteries. *Nanoscale* **2021**, *13*, 3937–3947. [[CrossRef](#)]

30. Casimir, A.; Zhang, H.; Ogoke, O.; Amine, J.C.; Lu, J.; Wu, G. Silicon-based anodes for lithium-ion batteries: Effectiveness of materials synthesis and electrode preparation. *Nano Energy* **2016**, *27*, 359–376. [[CrossRef](#)]
31. Chae, S.; Xu, Y.; Yi, R.; Lim, H.; Velickovic, D.; Li, X.; Li, Q.; Wang, C.; Zhang, J. A Micrometer-Sized Silicon/Carbon Composite Anode Synthesized by Impregnation of Petroleum Pitch in Nanoporous Silicon. *Adv. Mater.* **2021**, *33*, 2103095. [[CrossRef](#)] [[PubMed](#)]
32. Tu, W.; Bai, Z.; Deng, Z.; Zhang, H.; Tang, H. In-Situ Synthesized Si@C Materials for the Lithium Ion Battery: A Mini Review. *Nanomaterials* **2019**, *9*, 432. [[CrossRef](#)] [[PubMed](#)]
33. Wilson, A.M.; Way, B.M.; Dahn, J.R.; van Buuren, T. Nanodispersed silicon in pregraphitic carbons. *J. Appl. Phys.* **1995**, *77*, 2363–2369. [[CrossRef](#)]
34. Chan, C.K.; Peng, H.; Liu, G.; McIlwrath, K.; Zhang, X.F.; Huggins, R.A.; Cui, Y. High-performance lithium battery anodes using silicon nanowires. *Nat. Nanotechnol.* **2008**, *3*, 31–35. [[CrossRef](#)]
35. Cui, L.F.; Yang, Y.; Hsu, C.M.; Cui, Y. Carbon–silicon core–shell nanowires as high capacity electrode for lithium ion batteries. *Nano Lett.* **2009**, *9*, 3370–3374. [[CrossRef](#)]
36. Cui, L.-F.; Hu, L.; Choi, J.W.; Cui, Y. Light-Weight Free-Standing Carbon Nanotube-Silicon Films for Anodes of Lithium Ion Batteries. *ACS Nano* **2010**, *4*, 3671–3678. [[CrossRef](#)]
37. Choi, J.W.; Hu, L.; Cui, L.; McDonough, J.R.; Cui, Y. Metal current collector-free freestanding silicon–carbon 1D nanocomposites for ultralight anodes in lithium ion batteries. *J. Power Sources* **2010**, *195*, 8311–8316. [[CrossRef](#)]
38. Hu, L.; Wu, H.; Gao, Y.; Cao, A.; Li, H.; McDough, J.; Xie, X.; Zhou, M.; Cui, Y. Silicon-Carbon Nanotube Coaxial Sponge as Li-Ion Anodes with High Areal Capacity. *Adv. Energy Mater.* **2011**, *1*, 523–527. [[CrossRef](#)]
39. Liu, N.; Wu, H.; McDowell, M.T.; Yao, Y.; Wang, C.; Cui, Y. A yolk-shell design for stabilized and scalable LIB alloy anodes. *Nano Lett.* **2012**, *12*, 3315–3321. [[CrossRef](#)]
40. Liu, N.; Lu, Z.; Zhao, J.; McDowell, M.T.; Lee, H.-W.; Zhao, W.; Cui, Y. A pomegranate-inspired nanoscale design for large-volume-change lithium battery anodes. *Nat. Nanotechnol.* **2014**, *9*, 187–192. [[CrossRef](#)]
41. Wu, H.; Chan, G.; Choi, J.W.; Yao, Y.; McDowell, M.T.; Lee, S.W.; Jackson, A.; Yang, Y.; Hu, L.; Cui, Y. Stable cycling of double-walled silicon nanotube battery anodes through solid-electrolyte interphase control. *Nat. Nanotechnol.* **2012**, *7*, 310–315. [[CrossRef](#)] [[PubMed](#)]
42. Lu, Z.; Liu, N.; Lee, H.-W.; Zhao, J.; Li, W.; Li, Y.; Cui, Y. Nonfilling Carbon Coating of Porous Silicon Micrometer-Sized Particles for High-Performance Lithium Battery Anodes. *ACS Nano* **2015**, *9*, 2540–2547. [[CrossRef](#)] [[PubMed](#)]
43. Li, Y.; Yan, K.; Lee, H.W.; Lu, Z.; Liu, N.; Cui, Y. Growth of conformal graphene cages on micrometre-sized silicon particles as stable battery anodes. *Nat. Energy* **2016**, *1*, 15029. [[CrossRef](#)]
44. Ko, M.; Chae, S.; Ma, J.; Kim, N.; Lee, H.-W.; Cui, Y.; Cho, J. Scalable synthesis of silicon-nanolayer-embedded graphite for high-energy lithium-ion batteries. *Nat. Energy* **2016**, *1*, 16113. [[CrossRef](#)]
45. Sun, Y.; Lopez, J.; Lee, H.-W.; Liu, N.; Zheng, G.; Wu, C.-L.; Sun, J.; Liu, W.; Chung, J.W.; Bao, Z.; et al. A Stretchable Graphitic Carbon/Si Anode Enabled by Conformal Coating of a Self-Healing Elastic Polymer. *Adv. Mater.* **2016**, *28*, 2455–2461. [[CrossRef](#)]
46. Chen, H.; Ling, M.; Hencz, L.; Ling, H.Y.; Li, G.; Lin, Z.; Liu, G.; Zhang, S. Exploring Chemical, Mechanical, and Electrical Functionalities of Binders for Advanced Energy-Storage Devices. *Chem. Rev.* **2018**, *118*, 8936–8982. [[CrossRef](#)]
47. Bresser, D.; Buchholz, D.; Moretti, A.; Varzi, A.; Passerini, S. Alternative binders for sustainable electrochemical energy storage—the transition to aqueous electrode processing and bio-derived polymers. *Energy Environ. Sci.* **2018**, *11*, 3096–3127. [[CrossRef](#)]
48. Ai, Q.; Fang, Q.; Liang, J.; Xu, X.; Zhai, T.; Gao, G.; Guo, H.; Han, G.; Ci, L.; Lou, J. Lithium-conducting covalent-organic-frameworks as artificial solid-electrolyte-interphase on silicon anode for high performance lithium ion batteries. *Nano Energy* **2020**, *72*, 104657. [[CrossRef](#)]
49. Pan, J.; Peng, H.; Yan, Y.; Bai, Y.; Yang, J.; Wang, N.; Dou, S.; Huang, F. Solid-state batteries designed with high ion conductive composite polymer electrolyte and silicon anode. *Energy Storage Mater.* **2021**, *43*, 165–171. [[CrossRef](#)]
50. Hou, G.; Cheng, B.; Yang, Y.; Du, Y.; Zhang, Y.; Li, B.; He, J.; Zhou, Y.; Yi, D.; Zhao, N.; et al. Multiscale Buffering Engineering in Silicon–Carbon Anode for Ultrastable Li-Ion Storage. *ACS Nano* **2019**, *13*, 10179–10190. [[CrossRef](#)]
51. Zhang, W.; Fang, S.; Wang, N.; Zhang, J.; Shi, B.; Yu, Z.; Yang, J. A compact silicon–carbon composite with an embedded structure for high cycling coulombic efficiency anode materials in lithium-ion batteries. *Inorg. Chem. Front.* **2020**, *7*, 2487–2496. [[CrossRef](#)]
52. Han, C.; Si, H.; Sang, S.; Liu, K.; Liu, H.; Wu, Q. Achieving fully reversible conversion in Si anode for lithium-ion batteries by design of pomegranate-like Si@C structure. *Electrochim. Acta* **2021**, *389*, 138736. [[CrossRef](#)]
53. Du, Y.; Yang, Z.; Yang, Y.; Yang, Y.; Jin, H.; Hou, G.; Yuan, F. Mussel-pearl-inspired design of Si/C composite for ultrastable lithium storage anodes. *J. Alloys Compd.* **2021**, *872*, 159717. [[CrossRef](#)]
54. Yoshio, M.; Wang, H.; Fukuda, K.; Umeno, T.; Dimov, N.; Ogumi, Z. Carbon-Coated Si as a Lithium-Ion Battery Anode Material. *J. Electrochem. Soc.* **2002**, *149*, A1598. [[CrossRef](#)]
55. Jang, J.; Kang, I.; Yi, K.-W.; Cho, Y.W. Highly conducting fibrous carbon-coated silicon alloy anode for lithium ion batteries. *Appl. Surf. Sci.* **2018**, *454*, 277–283. [[CrossRef](#)]
56. Ng, S.H.; Wang, J.; Wexler, D.; Chew, S.Y.; Liu, H.K. Amorphous Carbon-Coated Silicon Nanocomposites: A Low-Temperature Synthesis via Spray Pyrolysis and Their Application as High-Capacity Anodes for Lithium-Ion Batteries. *J. Phys. Chem. C* **2007**, *111*, 11131–11138. [[CrossRef](#)]

57. Li, H.; Huang, X.; Chen, L.; Wu, Z.; Liang, Y. A High Capacity Nano-Si Composite Anode Material for Lithium Rechargeable Batteries. *Electrochem. Solid State Lett.* **1999**, *2*, 547–549. [[CrossRef](#)]
58. Wang, K.; Pei, S.; He, Z.; Huang, L.-A.; Zhu, S.; Guo, J.; Shao, H.; Wang, J. Synthesis of a novel porous silicon microsphere@carbon core-shell composite via in situ MOF coating for lithium ion battery anodes. *Chem. Eng. J.* **2019**, *356*, 272–281. [[CrossRef](#)]
59. Li, W.; Peng, J.; Li, H.; Wu, Z.; Chang, B.; Guo, X.; Chen, G.; Wang, X. Architecture and performance of Si/C microspheres assembled by nano-Si via electro-spray technology as stability-enhanced anodes for lithium-ion batteries. *J. Alloys Compd.* **2022**, *903*, 163940. [[CrossRef](#)]
60. Dou, F.; Shi, L.; Chen, G.; Zhang, D. Silicon/Carbon Composite Anode Materials for Lithium-Ion Batteries. *Electrochem. Energy Rev.* **2019**, *2*, 149–198. [[CrossRef](#)]
61. Li, W.; Peng, J.; Li, H.; Wu, Z.; Huang, Y.; Chang, B.; Guo, X.; Chen, G.; Wang, X. Encapsulating Nanoscale Silicon inside Carbon Fiber as Flexible Self-Supporting Anode Material for Lithium-Ion Battery. *ACS Appl. Energy Mater.* **2021**, *4*, 8529–8537. [[CrossRef](#)]
62. Zhang, L.; Wang, C.; Dou, Y.; Cheng, N.; Cui, D.; Du, Y.; Liu, P.; Al-Mamun, M.; Zhang, S.; Zhao, H. A Yolk-Shell Structured Silicon Anode with Superior Conductivity and High Tap Density for Full Lithium-Ion Batteries. *Angew. Chem. Int. Ed.* **2019**, *58*, 8824–8828. [[CrossRef](#)] [[PubMed](#)]
63. Hu, L.; Luo, B.; Wu, C.; Hu, P.; Wang, L.; Zhang, H. Yolk-shell Si/C composites with multiple Si nanoparticles encapsulated into double carbon shells as lithium-ion battery anodes. *J. Energy Chem.* **2019**, *32*, 124–130. [[CrossRef](#)]
64. Huang, X.; Sui, X.; Yang, H.; Ren, R.; Wu, Y.; Guo, X.; Chen, J. HF-free synthesis of Si/C yolk/shell anodes for lithium-ion batteries. *J. Mater. Chem. A* **2018**, *6*, 2593–2599. [[CrossRef](#)]
65. Shen, X.; Tian, Z.; Fan, R.; Shao, L.; Zhang, D.; Cao, G.; Kou, L.; Bai, Y. Research progress on silicon/carbon composite anode materials for lithium-ion battery. *J. Energy Chem.* **2018**, *27*, 1067–1090. [[CrossRef](#)]
66. An, W.; Gao, B.; Mei, S.; Xiang, B.; Fu, J.; Wang, L.; Zhang, Q.; Chu, P.K.; Huo, K. Scalable synthesis of ant-nest-like bulk porous silicon for high-performance lithium-ion battery anodes. *Nat. Commun.* **2019**, *10*, 1447. [[CrossRef](#)]
67. Chen, S.; Chen, Z.; Xu, X.; Cao, C.; Xia, M.; Luo, Y. Scalable 2D Mesoporous Silicon Nanosheets for High-Performance Lithium-Ion Battery Anode. *Small* **2018**, *14*, 1703361. [[CrossRef](#)]
68. Xu, X.; Wu, F.; Yang, W.; Dai, X.; Wang, T.; Zhou, J.; Wang, J.; Guo, D. Silicon@Natural Nitrogen-Doped Biomass Carbon Composites Derived from “Silicon Tofu” as Green and Efficient Anode Materials for Lithium-Ion Batteries. *ACS Sustain. Chem. Eng.* **2021**, *9*, 13215–13224. [[CrossRef](#)]
69. Li, X.; Zhang, M.; Yuan, S.; Lu, C. Research Progress of Silicon/Carbon Anode Materials for Lithium-Ion Batteries: Structure Design and Synthesis Method. *Chemelectrochem* **2020**, *7*, 4289–4302. [[CrossRef](#)]
70. Li, L.; Deng, J.; Wang, L.; Wang, C.; Hu, Y.H. Boron-Doped and Carbon-Controlled Porous Si/C Anode for High-Performance Lithium-Ion Batteries. *ACS Appl. Energy Mater.* **2021**, *4*, 8488–8495. [[CrossRef](#)]
71. Chen, J.; Guo, X.; Gao, M.; Wang, J.; Sun, S.; Xue, K.; Zhang, S.; Liu, Y.; Zhang, J. Self-supporting dual-confined porous Si@c-ZIF@carbon nanofibers for high-performance lithium-ion batteries. *Chem. Commun.* **2021**, *57*, 10580–10583. [[CrossRef](#)] [[PubMed](#)]
72. Zeng, Y.; Huang, Y.; Liu, N.; Wang, X.; Zhang, Y.; Guo, Y.; Wu, H.-H.; Chen, H.; Tang, X.; Zhang, Q. N-doped porous carbon nanofibers sheathed pumpkin-like Si/C composites as free-standing anodes for lithium-ion batteries. *J. Energy Chem.* **2021**, *54*, 727–735. [[CrossRef](#)]
73. Muraleedharan Pillai, M.; Kalidas, N.; Zhao, X.; Lehto, V.P. Biomass-based silicon and carbon for lithium-ion battery anodes. *Front. Chem.* **2022**, *10*, 882081. [[CrossRef](#)] [[PubMed](#)]
74. Di, F.; Wang, N.; Li, L.; Geng, X.; Yang, H.; Zhou, W.; Sun, C.; An, B. Coral-like porous composite material of silicon and carbon synthesized by using diatomite as self-template and precursor with a good performance as anode of lithium-ions battery. *J. Alloys Compd.* **2021**, *854*, 157253. [[CrossRef](#)]
75. Qi, C.; Li, S.; Yang, Z.; Xiao, Z.; Zhao, L.; Yang, F.; Ning, G.; Ma, X.; Wang, C.; Xu, J.; et al. Suitable thickness of carbon coating layers for silicon anode. *Carbon* **2022**, *186*, 530–538. [[CrossRef](#)]
76. Zhou, S.; Fang, C.; Song, X.; Liu, G. The influence of compact and ordered carbon coating on solid-state behaviors of silicon during electrochemical processes. *Carbon Energy* **2020**, *2*, 143–150. [[CrossRef](#)]
77. Zhang, Y.; Pan, Y.; Chen, Y.; Lucht, B.L.; Bose, A. Towards reducing carbon content in silicon/carbon anodes for lithium ion batteries. *Carbon* **2017**, *112*, 72–78. [[CrossRef](#)]
78. Azam, M.A.; Safie, N.E.; Ahmad, A.S.; Yuza, N.A.; Zulkifli, N.S.A. Recent advances of silicon, carbon composites and tin oxide as new anode materials for lithium-ion battery: A comprehensive review. *J. Energy Storage* **2021**, *33*, 102096. [[CrossRef](#)]
79. Ma, Q.; Dai, Y.; Wang, H.; Ma, G.; Guo, H.; Zeng, X.; Tu, N.; Wu, X.; Xiao, M. Directly conversion the biomass-waste to Si/C composite anode materials for advanced lithium ion batteries. *Chin. Chem. Lett.* **2021**, *32*, 5–8. [[CrossRef](#)]
80. Peng, J.; Li, W.; Wu, Z.; Li, H.; Zeng, P.; Chen, G.; Chang, B.; Zhang, X.; Wang, X. Si/C composite embedded nano-Si in 3D porous carbon matrix and enwound by conductive CNTs as anode of lithium-ion batteries. *Sustain. Mater. Technol.* **2022**, *32*, e00410. [[CrossRef](#)]
81. Chen, S.; Zheng, S.; Shi, A.; Zheng, L.; Zhang, Y.; Wang, Z. Distinctive conductivity improvement by embedding Cu nanoparticles in the carbon shell of submicron Si@C anode materials for LIBs. *Sustain. Energ. Fuel.* **2022**, *6*, 2306–2313. [[CrossRef](#)]
82. Mu, T.; Lou, S.; Holmes, N.G.; Wang, C.; He, M.; Shen, B.; Lin, X.; Zuo, P.; Ma, Y.; Li, R.; et al. Reversible Silicon Anodes with Long Cycles by Multifunctional Volumetric Buffer Layers. *ACS Appl. Mater. Interfaces* **2021**, *13*, 4093–4101. [[CrossRef](#)] [[PubMed](#)]

83. Luo, H.; Wang, Q.; Wang, Y.; Xu, C.; Wang, B.; Wang, M.; Wu, H.; Zhang, Y. Nano-silicon embedded in MOFs-derived nitrogen-doped carbon/cobalt/carbon nanotubes hybrid composite for enhanced lithium ion storage. *Appl. Surf. Sci.* **2020**, *529*, 147134. [[CrossRef](#)]
84. Wu, S.J.; Wu, Z.H.; Fang, S.; Qi, X.P.; Yu, B.; Yang, J.Y. A comparison of core-shell Si/C and embedded structure Si/C composites as negative materials for lithium-ion batteries. *Rare Met.* **2021**, *40*, 2440–2446. [[CrossRef](#)]
85. Kwon, H.J.; Hwang, J.-Y.; Shin, H.-J.; Jeong, M.-G.; Chung, K.Y.; Sun, Y.-K.; Jung, H.-G. Nano/Microstructured Silicon–Carbon Hybrid Composite Particles Fabricated with Corn Starch Biowaste as Anode Materials for Li-Ion Batteries. *Nano Lett.* **2019**, *20*, 625–635. [[CrossRef](#)]
86. Huang, S.; Shan, W.; He, S.; Chen, H.; Qin, H.; Wang, S.; Hou, X. Scalable Synthesis of Si/C Microspheres with 3D Conducting Nanosized Porous Channels as High-Performance Anodes in LIBs. *Energ. Fuel.* **2020**, *34*, 13137–13143. [[CrossRef](#)]
87. Zhu, G.; Zhang, F.; Li, X.; Luo, W.; Li, L.; Zhang, H.; Wang, L.; Wang, Y.; Jiang, W.; Liu, H.K.; et al. Engineering the Distribution of Carbon in Silicon Oxide Nanospheres at the Atomic Level for Highly Stable Anodes. *Angew. Chem. Int. Ed.* **2019**, *58*, 6669–6673. [[CrossRef](#)]
88. Tian, Y.; An, Y.; Feng, J. Flexible and Freestanding Silicon/MXene Composite Papers for High-Performance Lithium-Ion Batteries. *ACS Appl. Mater. Interfaces* **2019**, *11*, 10004–10011. [[CrossRef](#)]
89. Hui, X.; Zhao, R.; Zhang, P.; Li, C.; Wang, C.; Yin, L. Low-temperature reduction strategy synthesized Si/Ti<sub>3</sub>C<sub>2</sub> MXene composite anodes for high-performance Li-ion batteries. *Adv. Energy Mater.* **2019**, *9*, 1901065. [[CrossRef](#)]
90. Yang, S.H.; Kim, J.K.; Jung, D.-S.; Kang, Y.C. Facile fabrication of Si-embedded amorphous carbon@graphitic carbon composite microspheres via spray drying as high-performance lithium-ion battery anodes. *Appl. Surf. Sci.* **2022**, *606*, 154799. [[CrossRef](#)]
91. Chen, W.; Liu, H.; Kuang, S.; Huang, H.; Tang, T.; Zheng, M.; Yu, X. In-situ low-temperature strategy from waste sugarcane leaves towards micro/meso-porous carbon network embedded nano Si-SiO<sub>x</sub>@C boosting high performances for lithium-ion batteries. *Carbon* **2021**, *179*, 377–386. [[CrossRef](#)]
92. Zhenjie, L.I.; Du Zhong, J.Z.; Jinwei, C.; Gang, W.; Ruilin, W. Silicon nanoparticles/carbon composites for lithium-ion battery. *Prog. Chem.* **2019**, *31*, 201.
93. Wang, W.; Gu, L.; Qian, H.; Zhao, M.; Ding, X.; Peng, X.; Sha, J.; Wang, Y. Carbon-coated silicon nanotube arrays on carbon cloth as a hybrid anode for lithium-ion batteries. *J. Power Sources* **2016**, *307*, 410–415. [[CrossRef](#)]
94. Han, P.; Sun, W.; Li, D.; Luo, D.; Wang, Y.; Yang, B.; Li, C.; Zhao, Y.; Chen, L.; Xu, J.; et al. Morphology-controlled synthesis of hollow Si/C composites based on KI-assisted magnesiothermic reduction for high performance Li-ion batteries. *Appl. Surf. Sci.* **2019**, *481*, 933–939. [[CrossRef](#)]
95. Tang, H.; Xu, Y.; Liu, L.; Zhao, D.; Zhang, Z.; Wu, Y.; Zhang, Y.; Liu, X.; Wang, Z. A Hollow Silicon Nanosphere/Carbon Nanotube Composite as an Anode Material for Lithium-Ion Batteries. *Coatings* **2022**, *12*, 1515. [[CrossRef](#)]
96. Chen, H.; He, S.; Hou, X.; Wang, S.; Chen, F.; Qin, H.; Xia, Y.; Zhou, G. Nano-Si/C microsphere with hollow double spherical interlayer and submicron porous structure to enhance performance for lithium-ion battery anode. *Electrochim. Acta* **2019**, *312*, 242–250. [[CrossRef](#)]
97. Li, B.; Li, S.; Jin, Y.; Zai, J.; Chen, M.; Nazakat, A.; Zhan, P.; Huang, Y.; Qian, X. Porous Si@C ball-in-ball hollow spheres for lithium-ion capacitors with improved energy and power densities. *J. Mater. Chem. A* **2018**, *6*, 21098–21103. [[CrossRef](#)]
98. Wang, J.; Wang, Y.; Jiang, Q.; Zhang, J.; Yin, H.; Wang, Z.; Gao, J.; Wu, Z.; Liang, J.; Zuo, S. Interconnected Hollow Si/C Hybrids Engineered by the Carbon Dioxide-Introduced Magnesiothermic Reduction of Biosilica from Reed Plants for Lithium Storage. *Energ. Fuel.* **2021**, *35*, 10241–10249. [[CrossRef](#)]
99. Jiang, H.; Wang, S.; Shao, Y.; Wu, Y.; Shen, J.; Hao, X. Hollow Triple-Layer Puff-like HCs@Si@C Composites with High Structural Stability for High-Performance Lithium-Ion Battery. *ACS Appl. Energy Mater.* **2019**, *2*, 896–904. [[CrossRef](#)]
100. Zhang, J.; Zuo, S.; Wang, Y.; Yin, H.; Wang, Z.; Wang, J. Scalable synthesis of interconnected hollow Si/C nanospheres enabled by carbon dioxide in magnesiothermic reduction for high-performance lithium energy storage. *J. Power Sources* **2021**, *495*, 229803. [[CrossRef](#)]
101. Liu, X.; Shen, C.; Lu, J.; Liu, G.; Jiang, Y.; Gao, Y.; Li, W.; Zhao, B.; Zhang, J. Graphene bubble film encapsulated Si@C hollow spheres as a durable anode material for lithium storage. *Electrochim. Acta* **2020**, *361*, 137074. [[CrossRef](#)]
102. Liu, R.; Shen, C.; Dong, Y.; Qin, J.; Wang, Q.; Iocozzia, J.; Zhao, S.; Yuan, K.; Han, C.; Li, B.; et al. Sandwich-like CNTs/Si/C nanotubes as high performance anode materials for lithium-ion batteries. *J. Mater. Chem. A* **2018**, *6*, 14797–14804. [[CrossRef](#)]
103. Zhu, R.; Li, L.; Wang, Z.; Zhang, S.; Dang, J.; Liu, X.; Wang, H. Adjustable Dimensionality of Microaggregates of Silicon in Hollow Carbon Nanospheres: An Efficient Pathway for High-Performance Lithium-Ion Batteries. *ACS Nano* **2021**, *16*, 1119–1133. [[CrossRef](#)] [[PubMed](#)]
104. Man, Q.; An, Y.; Liu, C.; Shen, H.; Xiong, S.; Feng, J. Interfacial design of silicon/carbon anodes for rechargeable batteries: A review. *J. Energy Chem.* **2023**, *76*, 576–600. [[CrossRef](#)]

**Disclaimer/Publisher’s Note:** The statements, opinions and data contained in all publications are solely those of the individual author(s) and contributor(s) and not of MDPI and/or the editor(s). MDPI and/or the editor(s) disclaim responsibility for any injury to people or property resulting from any ideas, methods, instructions or products referred to in the content.